Research Article | Vol. 30, No. 7 / 28 Mar 2022 / Optics Express 11384
Optics EXPRESS

Inverse design assisted coherent optical lattices

DMITRY KOUZNETSOV,[1,2,3] ONGUN ARISEV,[1,2] POL VAN DORPE,[1,2] AND NIELS VERELLEN[2,4]

[1]KU Leuven, Dept. of Physics and Astronomy, Research unit Quantum Solid-State Physics, B- 3001 Leuven, Belgium
[2]imec, Kapeldreef 75, B- 3001 Leuven, Belgium
[3]dmitry.kouznetsov@imec.be
[4]niels.verellen@imec.be

Abstract: We explore the use of inverse design methods for the generation of periodic optical patterns in photonic integrated circuits. A carefully selected objective function based on the integer lattice method, which is an algebraic technique for optical lattice generation, is shown to be key for successful device design. Furthermore, we present a polychromatic pattern generating device that switches between optical lattices with different symmetry and periodicity depending on the operating wavelength. Important links are drawn between optical coherent lattices and optical potentials, pointing towards practical applications in the fields of quantum simulations and computing, optical trapping, and bio-sensing.

1. Introduction

Structured interference patterns of coherent waves, known as *coherent lattices*, play a key role in a wide range of applications. In particular, coherent lattices are prominent in structured illumination microscopy [1–3], fabrication of microstructures such as photonic [4] or plasmonic crystals [5], optical trapping in the life sciences [6] and quantum research [7,8]. Typically, an optical lattice is formed by the interference of counter-propagating laser beams, creating a spatially periodic pattern of focal spots. In our recent work we established a theoretical framework for generating diffraction limited multi-focal spot arrays with arbitrary periodicity, based on an integer lattice method [9]. This framework is particularly suitable for implementations in planar systems such as Photonic Integrated Circuits (PICs), which in recent years have come to the forefront as the platform of choice for novel photonics applications. However, the theoretical framework requires coordination of parallel wavefronts over a possibly large slab waveguide area where the pattern will be generated. Obtaining a parallel, i.e. non-diffracting, slab wavefront is nontrivial. Typically a large design footprint is required by e.g. linear tapers [10]. Thus, both the realization of the interference patterns and the attempt to keep the PIC design routing footprint small, pose a challenge.

Inverse design (InvDes) methods are a novel solution in the PIC community that allows to specify performance targets and manufacturing constraints in order to generate devices with arbitrary geometry, yet extremely small footprint and high efficiency [11–15]. Current InvDes strategies focus on making existing individual photonic components more compact, efficient and tolerant against manufacturing defects. Examples include compact planar waveguide tapers [16], beamsplitters [17] and vertical incidence grating couplers [18]. Starting from a general device blueprint and several design constraints, the method can automatically find optimal geometries that fulfill the specified performance criteria. In this work, we apply the InvDes method to the design of a PIC device capable of generating a coherent optical lattice (Fig. 1(c)) with minimal footprint. The structure shown in Fig. 1(d) is the three-dimensional render of such a device, demonstrating its compactness compared to a classical taper design.

#455466 https://doi.org/10.1364/OE.455466
Journal © 2022 Received 2 Feb 2022; revised 1 Mar 2022; accepted 1 Mar 2022; published 21 Mar 2022

Optics EXPRESS

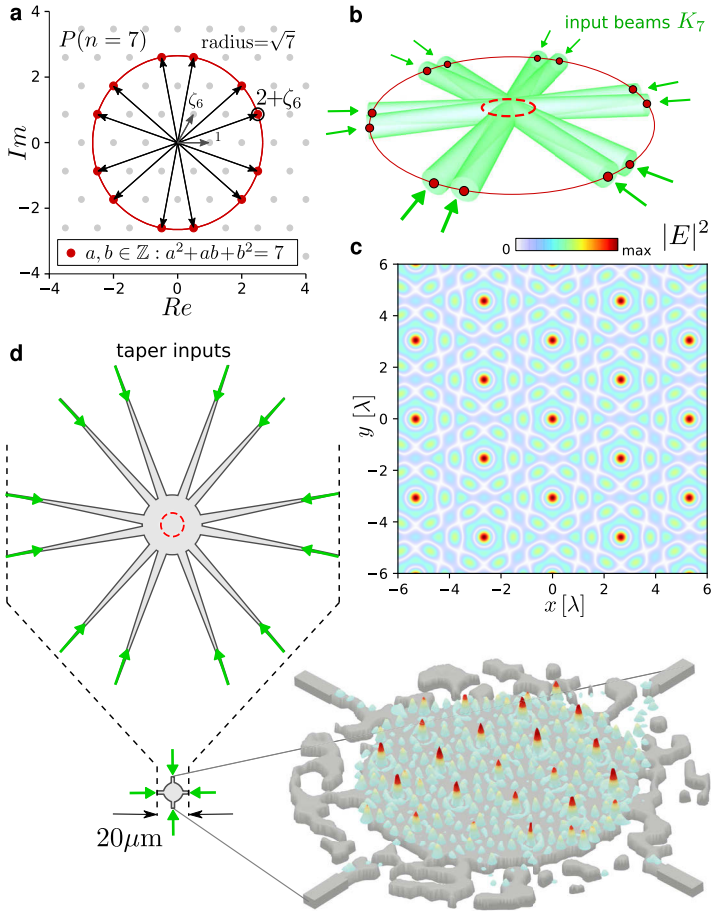

Fig. 1. Generation of optical lattices in a PIC using the integer lattice method. The wavevector components for the specific pattern are selected from concyclic points in the triangular integer lattice (a). Associating each wavevector with an input laser beam (b) produces the optical interference pattern in the overlapping region (c), denoted by a red dashed circle. The resulting device when setting the interference pattern as the target for the InvDes optimization (d) is shown to be more compact compared to the straight-forward linear taper design. The 12 plane wave inputs provided by the linear tapers are encoded in the InvDes device such that a mere 4 input waveguides suffice to generate the desired optical lattice.

We perform a gradient-based optimization of the PIC device using the adjoint method [19,20]. This technique allows the gradient of an objective function to be computed with respect to a large number of degrees of freedom, which is ideal for the design challenge at hand. Our key finding is that deriving the objective function from the electric field distribution (Fig. 1(c)) obtained from the integer lattice method for generating coherent optical lattices [9] is paramount for the convergence of the optimization to the final device design (Fig. 1(d)). The carefully selected objective function and subsequent tuning of the hyperparameters of the InvDes algorithm produces device designs that have the desired optical pattern and have a routing footprint that is nearly 100 times more compact than a conventional design approach.

All patterns are achieved without changing the topology of the central interference region (dashed red circles in Fig. 1(b,d)), such that it remains flat and homogeneous and could serve

Optics EXPRESS

as a platform for placing particles or other samples. In that case, the evanescent field of the optical lattices could enable bio-sensing or play the role of a trapping potential. We then also demonstrate that for successful design of PIC components that would produce optical coherent lattices a description of the underlying physics is crucial. This stands in contrast to the InvDes ethos of being able to directly design performant devices, not by having full understanding of the system, but by an optimization algorithm.

2. Formulation

Before setting up the InvDes problem for the photonic device, we will describe the device geometry used to generate optical lattice patterns in two-dimensions (2D) and define the constrains on the pattern selection posed by the algebraic integer lattice method [9]. In general, multiple input beams entering a central dielectric slab region will generate a 2D optical pattern due to interference (Fig. 1(b)). Any pattern generated in this way extends in the lower refractive index environment above the slab region as an evanescent electromagnetic field. Structuring this evanescent field is the key element in unlocking new integrated photonic device applications.

The integer lattice method relies on plane wave interference, where each plane wave light beam is associated with a wavevector. We restrict the discussion to a 2D geometry, which is suitable for PIC devices. We further assume that all input beams have transverse-electric polarization, which have only nonzero out-of-plane field components, and have equal relative intensity. The time-averaged intensity I of the electromagnetic field E is given by

$$I \propto |E|^2 = \left| E_0 \sum_{\mathbf{k}_j \in K_n} e^{-i\mathbf{k}_j \cdot \mathbf{r}} \right|^2, \tag{1}$$

where $\mathbf{r}$ is the position vector in two dimensions, E_0 is the overall field strength and K_n is a set of wavevector orientations which determine the optical pattern. In order to obtain optical lattices with specific symmetry and periodicity, K_n must be chosen carefully.

In Ref. [9], we demonstrated using a number theoretical approach that a planar (quasi-)periodic optical lattice can be constructed from the following set of wavevector orientations:

$$P(n) = \{N(\alpha) = n \mid \alpha \in \mathbb{Z}[\zeta_m]\}, \tag{2}$$

where the ring $\mathbb{Z}[\zeta_m] = \{a + b\zeta_m \mid a, b \in \mathbb{Z}\}$ determines the symmetry of the system fixed by choice of integer m in $\zeta_m = e^{2\pi i/m}$. The corresponding field norm $N(\alpha) = \alpha\bar{\alpha} = n$ then selects only specific wavevectors with an integer magnitude n. However, the set $P(n)$ in Eq. (2) contains only complex numbers (Fig. 1(a)) and therefore, to give physical meaning to these elements, here, we establish the set

$$K_n = \frac{2\pi}{\lambda} \mathrm{vec}\left(\frac{P(n)}{\sqrt{n}}\right), \tag{3}$$

where $\mathrm{vec} : x + yi \mapsto (x, y)$ simply converts the complex number to vector notation. Thus, concyclic points $P(n)$ in the complex plane (Fig. 1(a)) can be translated to orientations of the input beams (Fig. 1(b)), which in turn produce an optical lattice in the overlapping region (Fig. 1(c)). Note that the points $P(n)$ are normalized to have unit length and are subsequently scaled by the wavelength λ.

Setting the symmetry by choosing m and selecting a set K_n will result in an interference pattern according to Eq. (1). These are the coherent optical lattices and will be labeled $\Lambda_m(K_n)$.

Choice of Objective Function – When performing inverse design of a photonic device, the optimization over the parameter space relies on a good choice of a figure of merit (FOM) that characterizes the performance of the device while other system parameters are being varied. In our case, the spatial distribution of the electromagnetic field needs to match a target probe optical

Optics EXPRESS

lattice under variation of the material's dielectric constant. This also implies that a successful optimization will strongly rely on the initial choice of the geometry and the parameterization of the geometry, such that the FOM can be defined on the device.

For each device, we seek to maximize the FOM with respect to the permittivity distribution within a fixed design region. Since the optical lattices have rotational symmetry, the natural choice for the design region $\mathcal{D}$ is a annular shape surrounding the center slab region C (Fig. 2(a)). Next, we note that each optical lattice $\Lambda_m(K_n)$ is formed by a unique set of wavevectors K_n, which correspond to orientations of the input beams. Directly copying these orientations to determine the source positions for any non-trivial patterns would result in a large number of input waveguides being attached to the design region. For example, K_7 is a set of 12 wavevectors, as illustrated in Fig. 1(b). Instead, we can rely on the InvDes optimization to shape the permittivity distribution in the design region, routing the required wavevector components to form the desired pattern in the central slab region. To ensure that the radiation is distributed evenly with a manageable number of sources, we place four input waveguides around the design region, as shown in Fig. 2(a). By aligning these sources with the simulation coordinate grid, we gain the additional benefit of preventing any numerical errors in computing the mode residing in the input waveguides.

Having set the geometry of the optimization problem, our objective is to maximize the overlap integral of the generated electric field $\mathbf{E}$ and a target probe field $\mathbf{E}_{probe}$ within the central region C, representing a dielectric slab region where the desired pattern would be formed:

$$\max_{\boldsymbol{\epsilon}_r}(\text{FOM}) = \max_{\boldsymbol{\epsilon}_r} \int_C |\mathbf{E}^* \mathbf{E}_{probe}| \mathrm{d}\mathbf{r}, \tag{4}$$

where $\boldsymbol{\epsilon}_r$ is the relative permittivity distribution in the design region $\mathcal{D}$. For the optimization process, we use the finite-difference frequency-domain (FDFD) method to solve for the electric field distribution in the structure determined by a relative permittivity distribution. Then, we use a gradient ascent algorithm to perform updates of the design variables such that the integral in Eq. (4) is maximized with respect to $\boldsymbol{\epsilon}_r$ in the design region. This procedure is repeated until convergence on a final structure is reached. Having specified the device design and the objective function (Eq. (4)), what remains is to define the representation of the device in terms of a parameterization scheme.

Device parameterization – Starting from the initial design (Fig. 2(a)), the device is parameterized by a 2D array of density values $\boldsymbol{\rho}$. As described in detail in Refs. [21,22], low-pass spatial filtering and projection techniques are typically applied during optimization to create binarized final structures with large, smoothed features that can be adjusted for nanofabrication constraints. The spatial low-pass filter is achieved by convoluting the density $\boldsymbol{\rho}$ with a disk-shaped blurring kernel $\mathbf{f}(\sigma)$ with radius σ. Subsequently applying a projection function to the filtered density results in a 2D array with values varying between 0 and 1, called the projected density

$$\bar{\boldsymbol{\rho}} = \frac{\tanh(\beta\eta) + \tanh(\beta[\mathbf{f}(\sigma) * \boldsymbol{\rho} - \eta])}{\tanh(\beta\eta) + \tanh(\beta[1 - \eta])}, \tag{5}$$

where η is the mid-point of the projection (typically chosen to be $1/2$), and β controls the strength of the projection, as illustrated in Fig. 2(b). The permittivity is recreated from the projected density by adjusting for the minimum and maximum permittivity (ϵ_{min} and ϵ_{max} respectively)

$$\boldsymbol{\epsilon}_r = \epsilon_{min} + (\epsilon_{max} - \epsilon_{min})\bar{\boldsymbol{\rho}}\,. \tag{6}$$

We can also employ the density distribution to further demote the formation of small disjoint structures that would complicate fabrication. To accomplish this, we modify our original FOM in Eq. (4) by including a penalization term when small features form. The penalty term is typically

Optics EXPRESS

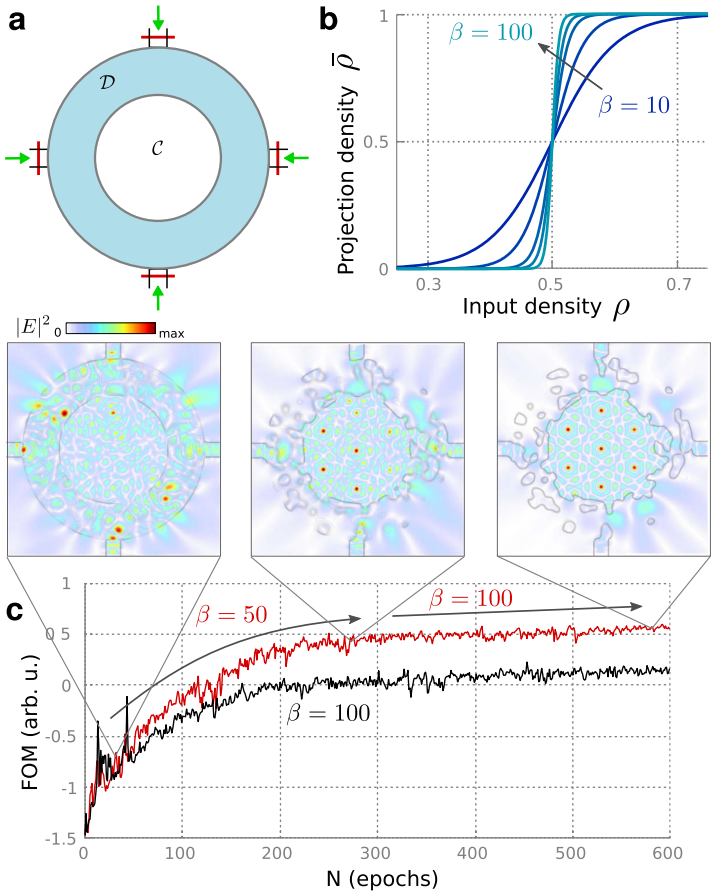

Fig. 2. Illustration of the important steps in the InvDes optimization. Pre-optimization blueprint of the device (a) with $\mathcal{C}$ the central interference region and $\mathcal{D}$ the design region being optimized. The four single mode input waveguides are indicated by arrows. (b) Plot of the projection function for binarization of the material. (c) β-parameter scheduling for each of the number of passes through the optimization steps (epochs) N. Scheduling the binarization into a weak and a strong phase shows an improvement in FOM maximization rate (red curve).

chosen to be proportional to the L^2-norm of the raw density array. The new objective function is then given by

$$\max_{\boldsymbol{\epsilon}_r} \int_{\mathcal{C}} \left(|\mathbf{E}^* \mathbf{E}_{probe}| - s|\boldsymbol{\rho}| \right) \mathrm{d}\mathbf{r}, \tag{7}$$

where s a number specifying the strength of the penalization. The exact implementation of the above steps can be found at the code repository we have made publicly available [23].

3. Results

To demonstrate the capabilities of our design approach, we solve the inverse design problem for prime examples of optical lattices with varying periodicity and symmetry. The starting structure for optimization consists of a central circular probe region and a surrounding ring-shaped design region with four input waveguides, as illustrated in Fig. 2(a). The single mode input beams with wavelength $\lambda = 1.5\,\mu\mathrm{m}$ are injected into a *Si* structure with permittivity $\epsilon_{Si} = \epsilon_{max} = 12$,

Optics EXPRESS

while the surrounded structure is Air, i.e. $\epsilon_{min} = 1$. The size of both the probe and the design region can be selected on a case-by-case basis, with the caveat that larger devices take longer to simulate. For numerical accuracy, the grid resolution is chosen to be smaller than $\lambda/40$ for the smallest wavelength considered, ≈ 25 pixels per wavelength inside the highest index medium. For convenience, we have not used full field 3D simulations in the optimization sweeps. For a specific PIC technology platform, this can be done but is beyond the scope of the current work.

In order to have a good starting condition for the final binarization of the density, we split the optimization process into a weak binarization stage and a strong binarization stage. This technique is often used to knead the design region into a smooth precursor density distribution so as to promote faster convergence once the full design constraints are enabled [24,25]. In our case, this is done by scheduling the value of the β parameter in Eq. (5) during optimization. For example, splitting a 600 epochs optimization into a $\beta = 50$ weak binarization for 300 epochs and $\beta = 100$ binarization for the remaining 300 epochs shows significant improvement in convergence, as shown in Fig. 2(c).

It is worth noting that even though the theory of integer lattices relies on plane wave harmonic analysis, the simulated patterns were obtained using a fully vectorial method. This means that the inverse designed devices, in fact, generates plane wave components in the central region.

Convergence condition – Optical lattices are always accompanied by complex interstitial patterns (see e.g. the optical lattice in Fig. 1(c)). From the theory of the integer lattice method, only specific optical lattice configurations have diffraction limited spots with enough sideband suppression to be sufficiently distinct from the background interference pattern [9]. In mathematical set notation we can say that the (unique) optical lattices $\Lambda_m(K_n)$ are ordered according to values of the field norm n. For triangular lattices ($m = 6$), the first few lattices are ordered as follows:

$$\{(1, \Lambda_6(K_1)), (2, \Lambda_6(K_7)), (3, \Lambda_6(K_{13})), \ldots\} \ . \tag{8}$$

Suppose one requires an application specific periodicity of high intensity spots (red on the scalebar in the figures), one could simplify the target probe field $\mathbf{E}_{probe}$ to consist only of high intensity gaussian spots at the desired positions, hoping that the optimization algorithm converges to form the target pattern. However, even if the target lattice is setup by arranging gaussian spots in a grid, the resulting optical interference pattern is not guaranteed to form a lattice with discernible spots. This is to say, for example, a lattice generated from K_5 cannot be constructed to have periodicity between $\Lambda_6(K_1)$ and $\Lambda_6(K_7)$ in expression (8). This can be easily verified by noting that the diophantine equation in Eq. (2) cannot be fulfilled, i.e. $a^2 + ab + b^2 = 5$ has no integer solutions.

Since the FOM is simply a value that the gradient ascent algorithm optimizes for, and by no means guarantees convergence to a resolvable optical lattice, an auxiliary quality score must be employed. To assess the similarity of the pattern formed by the resulting device and the ideal lattice of gaussian spots we can introduce an arbitrary similarity index. The Haar wavelet-based perceptual similarity index (HaarPSI) is a measure for images that aims to correctly assess the perceptual similarity between two images with respect to a human viewer [26]. The HaarPSI estimates local similarities between two images by computing coefficients obtained from a Haar wavelet decomposition. This similarity index was chosen based on its excellent performance for quantifying similarities between distorted images, as we have in our case.

When determining the HaarPSI index of optimized designs for increasing $\mathbf{E}_{probe}$ periodicity, we observe particular resonances for which the HaarPSI index shows better visual matching between the generated and target pattern. Each point in Fig. 3(e) starts from the same initial geometry (Fig. 2(a)), with the only variable being the distance d (i.e. periodicity) between spots in the target probe pattern (inset in Fig. 3(e)). The devices in Fig. 3(a-c) show convergence for the first three lattices according to expression (8). Devices targeting off-resonance periodicities do not converge to the desired pattern after an identical number of epochs (example pattern shown

Optics EXPRESS

in Fig. 3(d). For successful convergence of the optimization algorithm on the desired optical lattice, we found that the objective function should compute the overlap of the simulated electric field distribution and a chosen optical lattice as obtained by the integer lattice method.

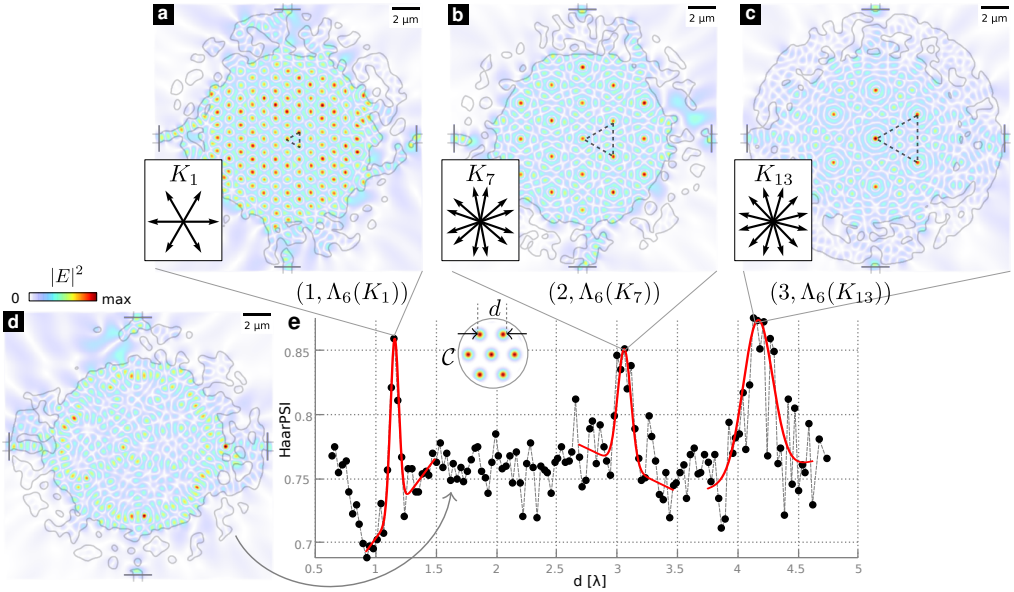

Fig. 3. Successful InvDes convergence to the target optical lattice is observed only for lattice periodicities that are a solution of the algebraic integer lattice method. Scanning the periodicities d of a grid of gaussian spots (inset (e)) reveals resonance peaks in the similarity index (HaarPSI) (e) exactly at the periodicities for the first three unique triangular optical lattices calculated using the integer lattice method (a-c). The inset arrow diagrams show the corresponding set of wavevectors to generate the target lattice. For lattices that have unfavorable periodicity, the optimization algorithm could not converge to the target (d). A gaussian fit to highlight the resonance locations is plotted (red lines (e)). Each data point represents an optimized device after 600 epochs ($N = 600$ in Fig. 2(c)).

Polychromatic Optical Lattices – As a final demonstration of the utility of the InvDes approach, we present the design of a device with wavelength-dependent generation of optical lattices. Specifically, we will target a bichromatic device that, depending on the input wavelength, toggles between a triangular and a rectangular optical lattice. To achieve such a device, the objective function needs to be modified to optimize for both target optical lattices with electric field distribution $\mathbf{E}_{probe,1}$ and $\mathbf{E}_{probe,2}$. It suffices to add the overlap integral for both wavelengths $\lambda_{1,2}$ such that the objective function becomes

$$\max_{\boldsymbol{\epsilon}_r} \int_C \left(|\mathbf{E}^*(\lambda_1)\mathbf{E}_{probe,1}| + |\mathbf{E}^*(\lambda_2)\mathbf{E}_{probe,2}| \right) \mathrm{d}\mathbf{r}, \tag{9}$$

where we left out the material penalty term (as in Eq. (7)) to save computational time.

In our specific example, a triangular optical lattice is formed when the input beams have a wavelength $\lambda = 1.5\,\mu\mathrm{m}$, and a square lattice for $\lambda = 1.3\,\mu\mathrm{m}$. The resulting device after optimization is shown in Fig. 4. We therefore show that it is possible to design devices that can generate optical lattices with both wavelength dependent symmetry and periodicity.

The number of patterns generated on a single device can be expanded, adding more colors to the FOM. However, the maximum number of simultaneous optical lattices that can be optimized for

Optics EXPRESS

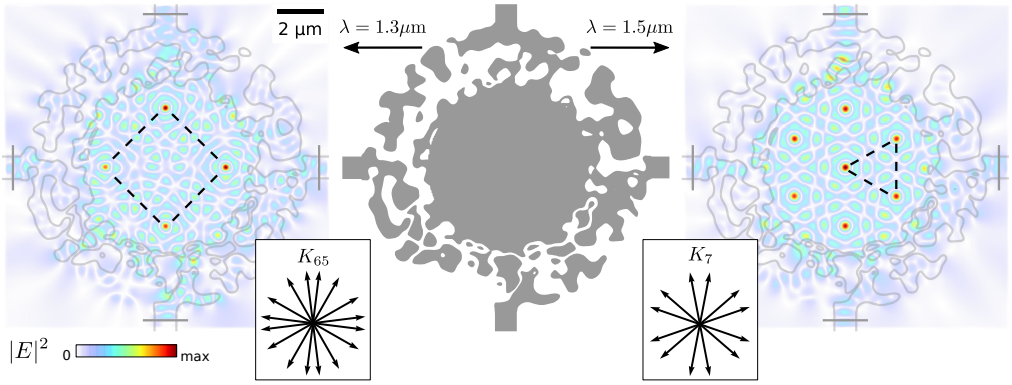

Fig. 4. Inverse design demonstration of a polychromatic optical lattice generating device. The final permittivity distribution after optimization is shown (center). When changing the operating wavelength in the four input waveguides, the generated optical lattice symmetry switches from square at $\lambda = 1.3\,\mu$m (left) to triangular at $\lambda = 1.5\,\mu$m (right). The inset diagrams show the corresponding set of wavevectors to generate the target optical lattices. The devices were obtained after an optimization for 2000 epochs.

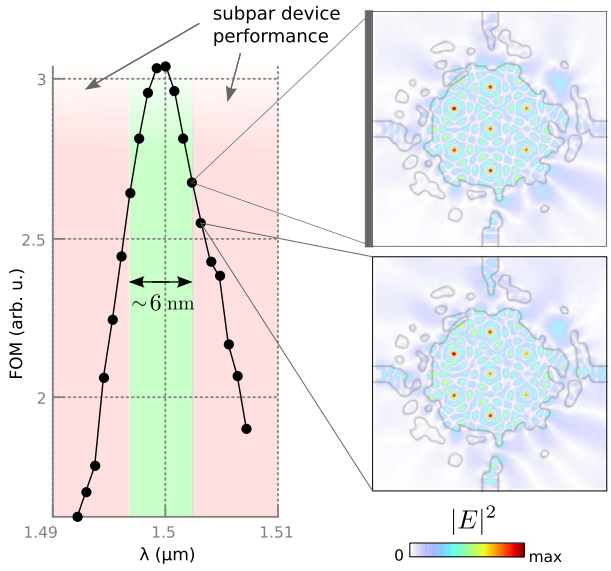

Fig. 5. Functional bandwidth of the optical pattern generating device. Wavelengths outside a 6 nm bandwidth showed significant degradation of the target pattern (regions shaded red). The quality threshold was set to FOM >2.6 based on a visual inspection of the device quality (intensity plots on the right).

Optics EXPRESS

depends on the available spectral band of the material platform. For example, in the 1.2 – 2.4 μm transparency range of the SOI platform, given a 0.2 μm buffer bandwidth per pattern as was set in the bichromatic example above, it is theoretically possible to fit 6 different optical lattice patterns. Squeezing in more patterns can be achieved by relaxing the optimization constraints, but this will likely interfere with the fabrication process ruleset.

Bandwidth analysis – It is important to analyze the robustness of the device w.r.t. the change in the operating wavelength. The functional bandwidth is determined to be ~ 6 nm by varying the input mode wavelength for a single device (Fig. 5). The functionality is much more sensitive compared to linear tapers (inputs in large structure in Fig. 2(d)), which can be broadband. Nevertheless, the device should be robust against variations in wavelength of an operating laser unit, and can thus be designed for the operational bandwidth.

4. Conclusion

In summary, we have shown that inverse design provides a practical means of efficiently designing compact PIC devices for the generation of structured illumination, and specifically optical lattices. For successful convergence of the optimization algorithm on a performant device, we found that the objective function should compute the overlap integral of the simulated electric field distribution and a chosen optical lattice that is a solution of the integer lattice method. Using our approach for silicon-on-insulator PIC devices, a wide range of optical lattice configurations were shown to be possible to design for. Next to triangular and square optical lattices, we also demonstrated polychromatic multi-pattern generation for a single device. The generated devices are designed to have a routing footprint 100 times more compact than the conventional linear taper approach.

The β and the penalty function in the FOM promote the binarization of the devices and constrain feature sizes, respectively. However, optimization may require additional sophisticated level-set methods for fabricable devices because the device is sensitive and resonant. For the given examples on SOI, the smallest feature sizes are in the range of tens of nanometers which can be achieved using e.g. electron beam lithography.

Our results continue the promising trend seen in the use of the inverse design approach to photonic device design, further illustrating the potential of these techniques to enable novel PIC applications. For example, the devices we presented can serve as optical trapping arrays for molecules or atoms at the high-intensity spot sites, and find applications in biosensing and PIC-based microscopy.

Funding. European Research Council (805222); Fonds Wetenschappelijk Onderzoek (1SC0321N).

Acknowledgments. We acknowledge grant support from FWO Vlaanderen (No. 1SC0321N) to D.K. This work is part of a project that has received funding from the European Research Council (ERC) under the European Union's Horizon 2020 research and innovation programme (Grant Agreement No. 805222).

Disclosures. The authors declare no conflicts of interest.

Data availability. Data underlying the results presented in this paper are available in Ref. [23].

References

1. M. G. Gustafsson, "Surpassing the lateral resolution limit by a factor of two using structured illumination microscopy," J. Microsc. **198**(2), 82–87 (2000).
2. E. Betzig, "Sparse and composite coherent lattices," Phys. Rev. A **71**(6), 063406 (2005).
3. A. G. York, S. H. Parekh, D. D. Nogare, R. S. Fischer, K. Temprine, M. Mione, A. B. Chitnis, C. A. Combs, and H. Shroff, "Resolution doubling in live, multicellular organisms via multifocal structured illumination microscopy," Nat. Methods **9**(7), 749–754 (2012).
4. M. Campbell, D. N. Sharp, M. T. Harrison, R. G. Denning, and A. J. Turberfield, "Fabrication of photonic crystals for the visible spectrum by holographic lithography," Nature **404**(6773), 53–56 (2000).
5. S. Kasture, A. P. Ravishankar, V. J. Yallapragada, R. Patil, N. V. Valappil, G. Mulay, and V. G. Achanta, "Plasmonic quasicrystals with broadband transmission enhancement," Sci. Rep. **4**(1), 5257 (2015).

Optics EXPRESS

6. A. Ashkin, J. M. Dziedzic, J. E. Bjorkholm, and S. Chu, "Observation of a single-beam gradient force optical trap for dielectric particles," Opt. Lett. **11**(5), 288 (1986).
7. M. Greiner, O. Mandel, T. Esslinger, T. W. Hänsch, and I. Bloch, "Quantum phase transition from a superfluid to a mott insulator in a gas of ultracold atoms," Nature **415**(6867), 39–44 (2002).
8. N. Mace, A. Jagannathan, and M. Duneau, "Quantum simulation of a 2d quasicrystal with cold atoms," Crystals **6**(10), 124 (2016).
9. D. Kouznetsov, Q. Deng, P. Van Dorpe, and N. Verellen, "Revival and Expansion of the Theory of Coherent Lattices," Phys. Rev. Lett. **125**(18), 184101 (2020).
10. G. T. Reed, *Silicon photonics: the state of the art* (John Wiley & Sons, 2008).
11. J. S. Jensen and O. Sigmund, "Topology optimization for nano-photonics," Laser & Photonics Rev. **5**(2), 308–321 (2011).
12. S. Molesky, Z. Lin, A. Y. Piggott, W. Jin, J. Vucković, and A. W. Rodriguez, "Inverse design in nanophotonics," Nat. Photonics **12**(11), 659–670 (2018).
13. P. R. Wiecha, A. Arbouet, C. Girard, and O. L. Muskens, "Deep learning in nano-photonics: inverse design and beyond," Photonics Res. **9**(5), B182–B200 (2021).
14. D. Liu, L. H. Gabrielli, M. Lipson, and S. G. Johnson, "Transformation inverse design," Opt. Express **21**(12), 14223–14243 (2013).
15. M. Burger, S. J. Osher, and E. Yablonovitch, "Inverse problem techniques for the design of photonic crystals," IEICE Trans. Electron. **87**, 258–265 (2004).
16. B. Luyssaert, P. Bienstman, P. Vandersteegen, P. Dumon, and R. Baets, "Efficient nonadiabatic planar waveguide tapers," J. Lightwave Technol. **23**(8), 2462–2468 (2005).
17. B. Shen, P. Wang, R. Polson, and R. Menon, "An integrated-nanophotonics polarization beamsplitter with $2.4 \times 2.4 \mu m^2$ footprint," Nat. Photonics **9**(6), 378–382 (2015).
18. A. Michaels and E. Yablonovitch, "Inverse design of near unity efficiency perfectly vertical grating couplers," Opt. Express **26**(4), 4766–4779 (2018).
19. M. B. Giles and N. A. Pierce, "An Introduction to the Adjoint Approach to Design," Flow, Turbul. Combust. **65**(3/4), 393–415 (2000).
20. T. W. Hughes, I. A. Williamson, M. Minkov, and S. Fan, "Forward-mode differentiation of maxwell's equations," ACS Photonics **6**(11), 3010–3016 (2019).
21. M. Zhou, B. S. Lazarov, F. Wang, and O. Sigmund, "Minimum length scale in topology optimization by geometric constraints," Comput. Methods Appl. Mech. Eng. **293**, 266–282 (2015).
22. T. W. Hughes, M. Minkov, I. A. D. Williamson, and S. Fan, "Adjoint method and inverse design for nonlinear nanophotonic devices," ACS Photonics **5**(12), 4781–4787 (2018).
23. D. Kouznetsov, O. Arisev, P. Van Dorpe, and N. Verellen, "Invdes optical lattice," Github (2021), https://github.com/dmitrykouznetsov/InvDes-Optical-Lattice.
24. D. Vercruysse, N. V. Sapra, L. Su, R. Trivedi, and J. Vučković, "Analytical level set fabrication constraints for inverse design," Sci. Rep. **9**(1), 8999 (2019).
25. Y. Augenstein and C. Rockstuhl, "Inverse design of nanophotonic devices with structural integrity," ACS Photonics **7**(8), 2190–2196 (2020).
26. R. Reisenhofer, S. Bosse, G. Kutyniok, and T. Wiegand, "A haar wavelet-based perceptual similarity index for image quality assessment," Signal Process. Image Commun. **61**, 33–43 (2018).